SOME FURTHER RESULTS FROM RUBBLE-PILE IMPACT CALCULATIONS. D. G. Korycansky, Erik Asphaug, *CODEP, Department of Earth and Planetary Sciences, University of California, Santa Cruz CA 95064*.

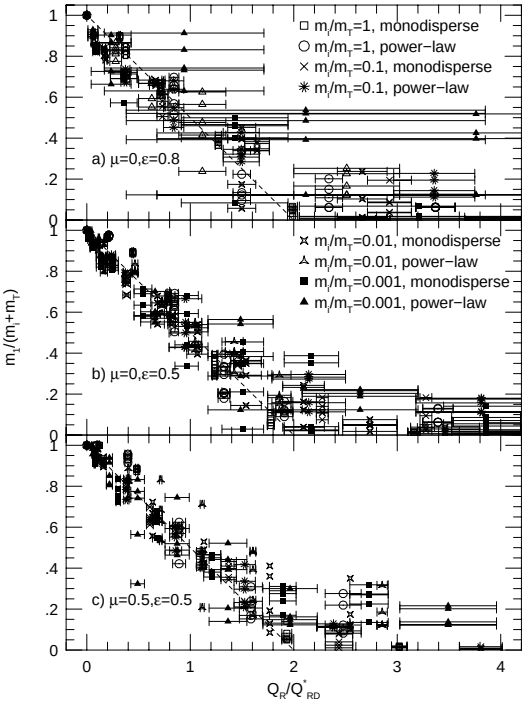

Figure 1: Mass ratio $m_1/(m_i+m_T)$ of largest fragment to total mass (impactor plus target) *vs.* ratio Q_R/Q^*_{RD} of reduced kinetic energy to critical reduced kinetic energy required to disrupt half the combined mass. Symbol types labeled in panels a) and b) hold for all three panels as indicated. Error bars reflect the effects of the variance in Q^*_{RD} as shown in Table 2. Panels a, b, c show low, medium and high-dissipation cases as labeled. The dashed line in each plot is the relation $m_1/(m_i+m_T) = 1 - Q_R/2Q^*_{RD}$.

In a recent paper, we report the results of some 1200 calculations of the impacts of km-scale rubble pile planetesimals [1]. The calculations were carried out using the Open Dynamics Engine (`www.ode.org`), a freely-available open-source "physics engine" that simulates rigid body motion and includes a sophisticated and fast collision detection method for non-spherical objects. Compared to our previous work [2,3], the use of ODE enables calculations to be run some 30 times faster. In our most recent paper, we carried out a parameter study of impacts involving ratios of impactor mass m_i to target mass m_T of $0.001 < m_i/m_T < 1$ and impact parameters $0 < b/b_0 < 0.866$, where b is scaled by the sum of the radii $b_0 = R_i + R_T$. Our main efforts focused on the determination of the so-called critical disruption energy Q^*_D, the kinetic energy per unit mass such that the mass of largest fragment m_1 equals half the target mass m_T. We found values of Q^*_D ranging from ~ 4 to 14 J kg^{-1} for low to high dissipation cases, where the dissipation was governed by the coefficients of friction μ and restitution ε. In this abstract we describe some results of additional analysis of our simulations.

Fragment mass scaling

Stewart and Leinhardt [4] have derived a new and different formulation criterion for catastrophic disruption that appears to collapse some of the ambiguity of the description, in particular the impactor/target mass ratio. Their description relies on relating the mass of the largest fragment to to total mass (impactor plus target), $m_i + m_T$ and a reduced kinetic energy $Q_R = (1/2)\tilde{\mu}v^2/(m_i+m_T) = Q^* m_T/(m_i+m_T)$ (in our notation). Stewart and Leinhardt propose the following relation: m_i/m_T

$$\frac{m_1}{m_i+m_T} = 1 - \frac{1}{2}\frac{Q_R}{Q^*_{RD}}, \qquad (1)$$

where Q^*_{RD} is the critical kinetic energy required such that $m_1 = (m_i+m_T)/2$. We calculated values for Q^*_{RD} for all our sets of head-on collisions with $n = 1000$-element targets. In Fig. 1 we plot all the runs according to the new variables suggested by Stewart and Leinhardt. It will be seen that the agreement with the relation Eqn. 2 is quite good, although a certain amount of scatter remains. The error bars reflect the range of our estimates Q^*_{RD} that comes about from the variance of the results, similar to that for Q^*_D. Interestingly, impacts with all three different levels of dissipation follow the relation. Some runs, particularly for small mass ratios and low dissipation, appear not to disrupt quite as easily as the relation would suggest, retaining some multi-body identity even at high energies (several times Q^*_{RD}, where Esq. 2 would suggest that targets would be completely shattered). Nevertheless, our results generally support the formulation suggested by Stewart and Leinhardt.

Fragment axis ratios

The distribution of shapes (axis ratios) of the aggregates resulting from collisions is also of interest. Although the velocities of the impacts are low (sub-km s^{-1} in all cases), it may be useful to compare the shapes the post-impact objects to the statistics of populations such as asteroids. Post-impact aggregates are held together by self-gravity and Coulomb friction that is applied during collisions among computational elements; there is no static friction or other cohesive force in play. We are interested in tracking shapes as a function of time with the object of determining how well our simulations are able to maintain non-spherical objects over long timescales in the face of numerical "jitter" due to non-zero timestep sizes that may induce relaxation to spherical shapes. Simulations were followed for 10^2 gravitational crossing times, or about 2.2×10^5 sec, with

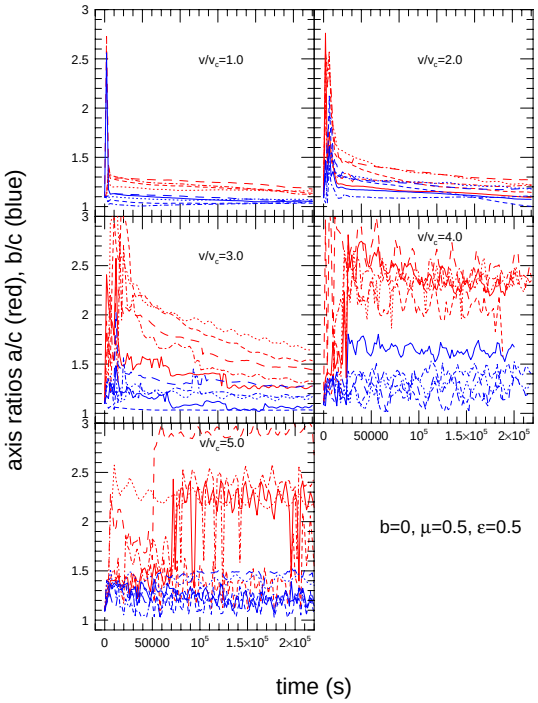

Figure 2: Axis ratios a/c, b/c, of the largest fragments m_1 as a function of time for $\mu = 0.5, \varepsilon = 0.5$ head-on collisions of equal-mass objects.

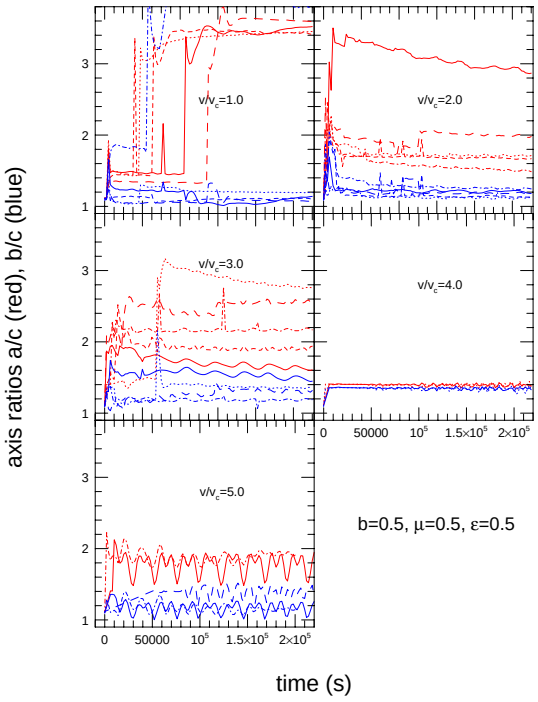

Figure 3: Axis ratios of the largest fragments m_1 as a function of time for $(\mu = 0.5, \varepsilon = 0.5)$ off-center $(b/b_0 = 0.5)$ collisions of equal-mass objects.

timesteps of 2 s, in general. We have processed the output of a subset of our calculations to determine axis ratios as measured by the moments of inertia of the post-collision objects and generated plots of axis ratios of post-impact as a function of time for a number of our simulations.

Fig. 2 shows the axis ratios a/c and b/c $(a > b > c)$ for a set of head-on collisions for our high-dissipation cases $(\mu = 0.5, \varepsilon = 0.5)$. Axis ratios are shown for the largest fragment m_1 after the collision. Red curves show axis ratio a/c, blue curves show b/c, where $a > b > c$ are the axes of the ellipsoid calculated from the moment of inertia tensor of m_1. Fig. 3 shows the same ratios for collisions that are mildly off-center (scaled impact parameter $b/b_0 = 0.5$). In general, in the aftermath of head-on collisions, axis ratios of m_1 show a trend toward decay toward spherical shapes, as seen in Fig. 2; higher-velocity collisions show both higher values and more stability of axis ratios, though it should be noted that the mass of m_1 is smaller for high-velocity impacts; fewer elements make up such fragments and it may be easier to maintain non-spherical shapes in those cases.

Off-axis collisions, as seen in Fig 3, have in general both larger and more stable axis ratios than head-on collisions. The lowest-speed collisions result in the coalescence of the initial impactor and target into one highly-elongated prolate object and are special cases. We have also analyzed our more highly off-axis collisions $(b/b_0 = 0.707,\ 0.866)$ and have found the same behavior. At this writing we are not sure of the cause of the difference between the outcomes of head-on and oblique collision simulations. It is possible that off-axis collisions give rise to more rapidly rotating post-impact objects for which rotational dynamics play a part in sustaining non-spherical shapes. Further analysis is needed to look for correlations between rotational states and object shapes in our calculations.

Overall we are cautiously encouraged by these outcomes; it seems likely that at least some moderately oblate or prolate shapes can be supported over significant timescales (hundreds of dynamical crossing times). An alternative way of stating this result is that non-trivial angles of repose can potentially be supported on rubble piles for long times by our simulation code. In turn this may enable the study of interesting long-term processes (such as Yarkovsky effects, e.g. YORP) that are increasingly thought to be important in solar system geophysics.

Acknowledgments

This work is supported by the NASA's Planetary Geology and Geophysics Program, under award NNX07AQ04G.

References

[1] Korycansky and Asphaug 2008, *Icarus*, submitted. [2] Korycansky 2004, *Astrophys. Space Sci.* **291**, 57. [3] Korycansky and Asphaug 2006, *Icarus* **181**, 605. [4] Stewart and Leinhardt 2008, *Astrophys. J. Lett.*, submitted.